

# Plasmon induced transparency and refractive index sensing in a new type of graphene-based plasmonic waveguide



Di Wu<sup>a</sup>, Jinping Tian<sup>a,b,\*</sup>, Lu Li<sup>a</sup>, Rongcao Yang<sup>a</sup>

<sup>a</sup> College of Physics and Electronic Engineering, Shanxi University, Taiyuan 030006, PR China

<sup>b</sup> College of Modern Education and Technology, Shanxi University, Taiyuan 030006, PR China

## ARTICLE INFO

### Keywords:

Plasmon induced transparency  
Graphene  
Refractive index sensor  
Figure of merit

## ABSTRACT

The plasmon induced transparency (PIT) effect is investigated in a graphene-based waveguide, which is composed of a graphene bus waveguide side-coupled with a graphene strip directly and a graphene ring indirectly. Conventional numerical simulations based on finite element method (FEM) are used to study the transmission properties through optimizing the relevant parameters, and it is proved that the simulation results agree well with the analytical results. Then as one of the potential application branches of the PIT-like effect, the property of refractive index sensing with a higher sensitivity of 4160 nm/RIU is further studied. The result can help to deepen the understanding of PIT-like effect and nano sensor, and it would be also beneficial for the studies and applications of nanoscale graphene-based optical devices.

© 2017 Elsevier B.V. All rights reserved.

## 1. Introduction

In recent years, the effect of quantum interference has become one of the research hot spots in the field of physics because many physical phenomena are generated in quantum optics and atomic physics, such as electromagnetically induced transparency (EIT) and electromagnetically induced absorption (EIA). The EIT is generated by quantum interference between pumping and probing field, which occurs in three-level atomic system [1,2]. Compared with the EIT in atomic systems, the plasmonic analogue of EIT or plasmon induced transparency (PIT) has attracted much attention due to its significant advantages and wide practical applications, such as sensor [3,4], active plasmonic switch [5,6], polarization conversion [7], and so on. However, most of these structures mentioned above are composed of metallic materials and in real application, it is often needed to change their geometrical parameters to realize the dynamic control of the PIT-like window, which significantly limit the scope of their applications. Meanwhile, not only the metallic structures will have larger propagation losses but also it will have difficulties in controlling the permittivity, and it will also result in a lower ability of active modulation. To overcome these shortcomings, many approaches have been focused on the structures using graphene material [8–11] in recent years to achieve dynamic tunability of PIT phenomenon.

Graphene, known as a type of two-dimensional material of which the carbon atoms are packed in honeycomb like crystal lattice [12,13],

has attracted particular attention in recent years due to its remarkable electronic and optical properties [14–16]. The latest research results show that enhanced performance of light-controlled conductive switching can be achieved in hybrid cuprous oxide/reduced graphene oxide (Cu<sub>2</sub>O/rGO) nanocomposites [17]. In [18], tunable photoluminescence of water-soluble AgInZnS-graphene oxide (GO) nanocomposites and their application in-vivo bioimaging are reported. It is well-known that in the mid-infrared and terahertz frequency ranges, graphene can be used as an alternative to the traditional noble-metal plasmonics. To excite the plasmons in graphene-based waveguide, the periodically patterned graphene structures [19], sub-wavelength dielectric gratings [20], have been used in the experiments. Compared with traditional noble metal materials working in visible and near infrared frequencies, graphene has some major advantages [21] such as low loss, extreme mode confinement capacity and dynamic tunability [10,11]. The stronger confinement of plasmons in graphene can create strong light-matter interactions and can be potentially used to build different types of optical devices. Moreover, in contrast to the noble metals, the most notable property of graphene is that its surface conductivity can be flexibly altered by either chemical doping or gate voltage [22–25] without refabricating the structure. Based on these unique characteristics, the graphene has certainly turned to be a very promising material for optical devices analogue to those using noble metals, including absorber [26], sensor [27] and PIT applications [10,28–30].

\* Corresponding author at: College of Modern Education and Technology, Shanxi University, Taiyuan 030006, PR China.

E-mail address: [tianjp@sxu.edu.cn](mailto:tianjp@sxu.edu.cn) (J. Tian).

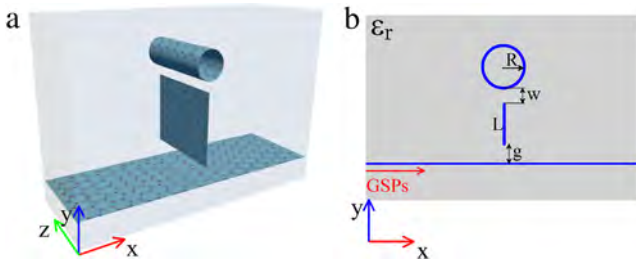


Fig. 1. (a) 3D schematic diagram and (b) Side view of the graphene-based PIT waveguide structure.

In [31], plasmon-induced absorption in a single graphene sheet with two air cavities side-coupled to a graphene nanoribbon is investigated. In [32], the authors demonstrated that PIT can be achieved by placing a flat monolayer graphene under a sinusoidally curved graphene layer. In [33], multi-mode PIT in dual graphene ring resonators is studied, and in [34], multicavity-coupled graphene-based waveguide system as well as its PIT transmission is demonstrated. In [35], the authors have theoretically investigated the PIT characteristics using coupled mode theory (CMT) in integrated graphene waveguides with direct and indirect couplings. Recently, Wang et al. investigated the Fano resonance and its sensing application in an improved grating-coupled graphene structure [36].

However, as far as we know, few results have been found for the research of PIT in a graphene-based waveguide coupled to a vertically placed graphene strip resonator except for Ref. [30], where the authors use two graphene sheets with finite length placed symmetrically on both sides of the graphene bus waveguide as two detuned side-coupled resonators to achieve the PIT-like phenomenon. However, the two resonators are both standing-wave (SW) cavity, and it is well-known that the couplings between a bus waveguide and a traveling-wave (TW) cavity or SW cavity are different [35]. Thus inspired by the special properties of graphene and the reported research results, this paper is to design a new type of graphene-based PIT waveguide system, where a vertical placed graphene strip is used as a resonator, and at the same time, it is side-coupled with a graphene ring on the top and with a graphene bus waveguide at the bottom. Meanwhile, the ring resonator works as a TW cavity while the strip resonator works as a SW cavity. Then in this paper, the effects of the structural parameters and chemical potential of the graphene on the transmission characteristics are studied in detail. In addition, the refractive index sensing performance based on the PIT-like effect is also to be calculated. This proposed compact plasmonic structure may pave a new way for the flexible and tunable PIT-like properties in the application of compact integrated photonic devices.

## 2. Geometry and theoretical model

The graphene-based waveguide system designed to demonstrate the PIT-like phenomenon is shown in Fig. 1. It consists of a graphene ring and a graphene bus waveguide with a vertical graphene strip placed in between. The graphene bus waveguide and strip can be made by chemical vapor deposition (CVD) method [37–39], and the graphene layer can tightly coat a dielectric nanowire due to van der Waals force [40] to form the ring resonator. The input optical power can only be coupled to the graphene ring indirectly through the near-field coupling with graphene strip. The length of graphene strip is  $L$ , the radius of graphene ring is  $R$ , the separation distance between the strip and the ring is  $w$ , and that between the strip and bus waveguide is  $g$ . The overall system is embedded in a background material with a relative permittivity of  $\epsilon_r$ . Graphene is treated as an ultra-thin two-dimensional material with a thickness of  $t = 0.5$  nm [41], because the surface conductivity of graphene remains constant when its effective thickness

varies, and the mode properties, i.e. the refractive index, are actually insensitive to the specific value of the thickness, as long as it is small enough. Its equivalent dielectric constant can be calculated by [42]:

$$\epsilon_g = 1 + \frac{i\sigma(\omega)}{\omega\epsilon_0 t} \quad (1)$$

where  $\omega$  is the frequency of the incident light,  $\epsilon_0$  is the vacuum dielectric constant,  $\sigma(\omega)$  is the surface conductivity of graphene, which can be expressed by the Kubo's formula [43]

$$\begin{aligned} \sigma(\omega) = & \frac{i2e^2k_B T}{\pi\hbar^2(\omega + i\tau^{-1})} \ln \left[ 2 \cosh \left( \frac{E_f}{2k_B T} \right) \right] \\ & + \frac{e^2}{4\hbar} \left[ \frac{1}{2} + \frac{1}{\pi} \tan^{-1} \left( \frac{\hbar\omega - 2E_f}{2k_B T} \right) \right] \\ & - \frac{i}{2\pi} \ln \frac{(\hbar\omega + 2E_f)^2}{(\hbar\omega + 2E_f)^2 + 4(k_B T)^2} \end{aligned} \quad (2)$$

where  $T = 300$  K is room temperature,  $k_B$  is the Boltzmann's constant,  $\hbar$  is the reduced Planck's constant, and  $e$  is the electron charge. The electron relaxation time is expressed as  $\tau = \mu E_f / eV_F^2$ , where  $V_F = c/300$  is the Fermi velocity,  $E_f$  is the chemical potential, and  $\mu = 2.0 \text{ m}^2/\text{Vs}$  is the DC mobility of graphene [41,44]. In our analysis, the incident light is assumed to be in the mid-infrared wavelength range where the intraband transition is dominant, and under this condition, the optical conductivity of monolayer graphene can be simplified as:

$$\sigma(\omega) = \frac{ie^2 E_f}{\pi\hbar^2(\omega + i\tau^{-1})} \quad (3)$$

In this paper, the chemical potentials of the graphene waveguide, graphene strip and graphene ring are respectively set as  $E_{f1}$ ,  $E_{f2}$  and  $E_{f3}$ . During the simulation, only the transverse magnetic (TM) polarized graphene surface plasmon (GSP) mode is considered throughout this paper. To excite the plasmon waves in practice in the real structure, one can refer to the method of Refs. [20,45,46]. The fundamental GSP mode is injected from the left side of the bus graphene waveguide. The transmission spectra and field distributions are simulated by the Comsol Multiphysics based on the finite element method (FEM), and the 2D-RF Module with perfectly matched layer (PML) absorbing boundary condition is used. Convergence tests are done in the processes of mesh generation to ensure the accuracy of the calculation. During simulation, non-uniform mesh is used and the mesh size in graphene layer is 0.1 nm, and extremely refined mesh size is used in other area.

It should be noted that in [35], PIT phenomenon using graphene strip resonators placed parallel to the bus waveguide is studied. But here, compared with the Refs. [8] and [35], a vertical graphene strip resonator is used in the structure. As we have found that the difficulty of manipulating the PIT effect will increase if the parallel graphene strip is used in the proposed structure. That is because it will increase the direct coupling between the graphene bus waveguide and the ring resonator even though the whole structure will become compact. What is more, according to the CMT [35,47], if one considers a waveguide composed of a bus waveguide side-coupled with only a ring resonator or a strip resonator, the transmission can be respectively written as

$$T_{ring} = \left| \frac{i(\omega - \omega_0) + \kappa_i - \kappa_e}{i(\omega - \omega_0) + \kappa_i + \kappa_e} \right|^2 \quad (4.1)$$

or

$$T_{strip} = \left| \frac{i(\omega - \omega_0) + \kappa_i}{i(\omega - \omega_0) + \kappa_i + \kappa_e} \right|^2 \quad (4.2)$$

where  $\omega_0$  is the resonant frequency,  $\kappa_i$  and  $\kappa_e$  are respectively decay rates due to intrinsic loss and waveguide coupling loss. Thus one will have the minimum transmission rates as  $T_{ring} = \left| \frac{\kappa_i - \kappa_e}{\kappa_i + \kappa_e} \right|^2$  and  $T_{strip} = \left| \frac{\kappa_i}{\kappa_i + \kappa_e} \right|^2$  when resonance occurs. Usually,  $\kappa_i \ll \kappa_e$  is always satisfied as long as the waveguide size is much smaller than the working wavelength, and then the minimum transmission  $T_{strip}$  is less than  $T_{ring}$ ,

which will present a good performance in real application. And thus a graphene strip resonator is to be used in this paper to study the transmission properties of the proposed waveguide structure.

### 3. Simulation and discussion

Before investigating the PIT characteristics of the proposed structure, we firstly calculated the dependence of the transmission spectrum on the incident wavelength when the upper graphene ring is absent. The result shown in Figs. 2(a) and (c) respectively represent the transmission spectrum when the background material is air and SiO<sub>2</sub>. The graphene strip lengths are respectively set as  $L = 280$  nm (black line),  $L = 300$  nm (red line) and  $L = 320$  nm (blue line) for comparison. The other parameters are  $E_{f1} = 0.4$  eV,  $E_{f2} = 0.5$  eV, and  $g = 50$  nm. It can be clearly found that there are two stopbands, which correspond to the first and second order resonance of the graphene strip respectively, appearing in the transmission spectra for the given wavelength range. Meanwhile, the spectra all red shifted with the increase of  $L$ . When the background medium is silica, the whole transmission spectrum moves to the long wavelength band, and the line widths (the full width at half maximum, FWHM) of the two stopbands are larger than that of using air as the background medium. These results can be explained in terms of the resonant condition of the graphene strip resonator, which can be deduced from the quasi-static analysis [48–50]

$$\lambda_p = \frac{2\pi\hbar c}{e} \sqrt{\frac{\epsilon_{eff}\epsilon_0\eta L}{E_f}} \quad (5)$$

here,  $L$  is the length of the graphene strip,  $c$  is the velocity of light in vacuum,  $\eta$  is an undetermined dimensionless fitting constant, and  $\epsilon_{eff} = (\epsilon_r + \epsilon_r)/2 = \epsilon_r$  is the effective permittivity of the medium surrounding the graphene strip. It can be obtained from Eq. (5) that  $\lambda_p \propto \sqrt{L}$  and  $\lambda_p \propto \sqrt{\epsilon_{eff}}$  are always satisfied, that is to say, the increase of the strip length  $L$  and permittivity  $\epsilon_r$  will lead to the redshift of the resonance wavelength. The dependences of the first- and second-order resonant dip wavelengths on the length of the graphene strip are respectively shown in Figs. 2(b) and (d) corresponding to Figs. 2(a) and (c). As is expected, the two dip wavelengths are linear with the strip length, and the simulation results agree well with the theoretical fitting results calculated by Eq. (5). The fitting parameter  $\eta$  in Fig. 2(b) is 2.675 or 1.139 for the first- or second-order transmission dips, and is 2.671 or 1.137 in Fig. 2(d). One can find that the fitting parameter is nearly equal for the same resonant order, and is almost independent on the surrounding medium of the waveguide structure.

It is known that the performance of a graphene-based waveguide is greatly affected by the GSP mode confinement and propagation length. When the SiO<sub>2</sub> with  $\epsilon_r = 2.09$  is used as the background medium, the real part of the effective index  $Re(neff) = Re(\beta)/k_0$  and the propagation loss will increase than the case of air background, and the maximum transmission rate will also decrease. Here  $\beta$  represents the propagation constant of GSP wave and  $k_0$  is the vacuum wavenumber. Figs. 3(a) and (b) show the propagation length  $L_p = 1/Im(\beta)$  and the effective index  $Re(neff)$  of the GSP mode. It can be found that the effective index will decrease with the increase of working wavelength, while the propagation length will increase with the increase of working wavelength, indicating a decreasing propagating loss. Meanwhile, the effective index in silica is larger than that in air while the propagation length is smaller. To sum up, one can find that the change of background medium will not affect the shape of the transmission spectra except for the locations of transmission dips and the line width of each stopband. So in order to simplify the numerical simulation, the background material is assumed to air in the rest of this paper [8,29,46,48]. When the background medium is set as air, the propagation constant  $\beta$  of the GSP wave along the suspended graphene sheet can be written as [22]:

$$\beta = k_0 \sqrt{1 - \left(\frac{2}{\eta_0\sigma}\right)^2} \quad (6)$$

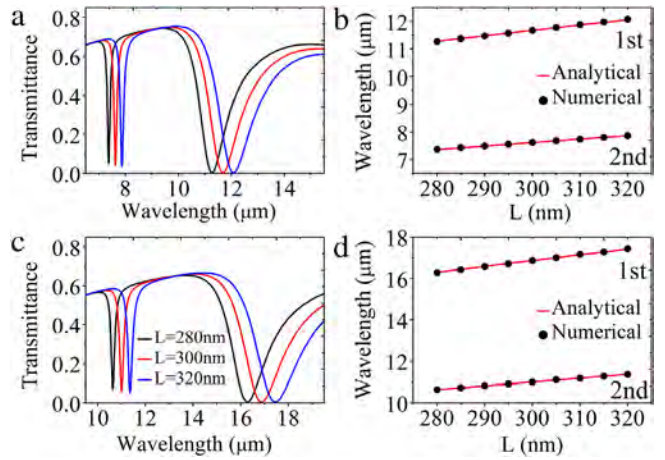


Fig. 2. (a) and (c) are respectively the transmission spectra for different graphene strip lengths when the upper graphene ring is absent. (b) and (d) are respectively the dependence of the first and second order resonant dip wavelengths on the length of the graphene strip. Black dots are simulation results and red line is theoretical result. The background medium is air in (a), (b) and is SiO<sub>2</sub> in (c), (d). Here,  $E_{f1} = 0.4$  eV,  $E_{f2} = 0.5$  eV,  $g = 50$  nm. (For interpretation of the references to color in this figure legend, the reader is referred to the web version of this article.)

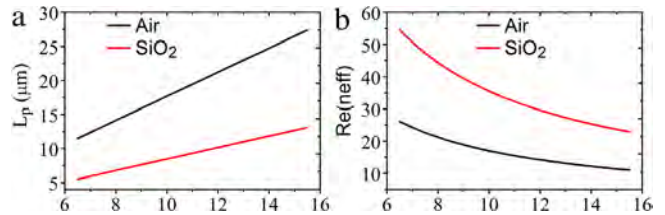


Fig. 3. (a) Effective index and (b) propagation length as a function of the incident wavelength for graphene sheet embedded in different background material.

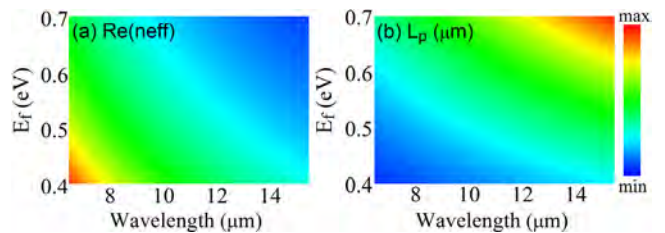
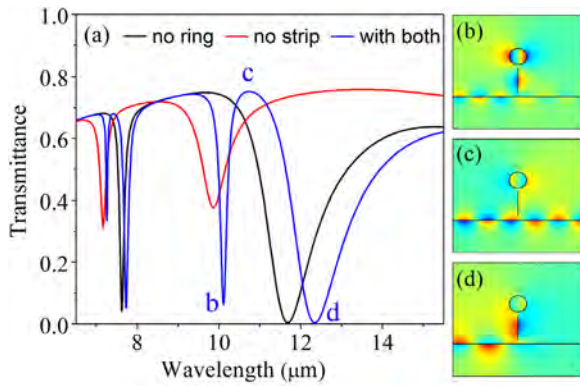


Fig. 4. (a) Real part of GSP effective index and (b) GSP propagation length as functions of working wavelength and chemical potential.

here,  $\eta_0 \approx 377 \Omega$  and  $k_0 = 2\pi/\lambda$  are respectively the impedance and the wavenumber in free space. The dependences of  $Re(neff)$  and  $L_p$  on the incident light wavelength and the chemical potential  $E_f$  using Eq. (6) are shown in Figs. 4(a) and (b). Obviously, one can find that for a fixed incident wavelength,  $Re(neff)$  increases with the decrease of the chemical potential  $E_f$ , which means that GSPs are better confined at a lower chemical potential and that a lower chemical potential will give a smaller propagation length. Thus, for the considered infrared frequency range, both these important factors should be taken into consideration in the design of PIT-like system. Interestingly, one can control the chemical potential of graphene by external gate voltage without changing the geometry of the structure, which provides a smart way to actively control the transmission properties of the proposed structure.

The PIT transmission spectrum of the proposed structure with  $E_{f1} = 0.4$  eV,  $E_{f2} = E_{f3} = 0.5$  eV,  $R = 100$  nm,  $L = 300$  nm,  $g = 50$  nm, and  $w = 40$  nm is shown in Fig. 5(a). For the aim of comparison, the transmission spectra of the structure with merely graphene strip



**Fig. 5.** (a) Transmission spectra without the graphene ring (black curve), without the graphene strip (red curve) and with both graphene ring and strip (blue curve). The distributions of the magnetic field component Hz corresponding to the points b, c, and d in (a) are shown in (b)  $\lambda = 10.11 \mu\text{m}$ , (c)  $\lambda = 10.73 \mu\text{m}$ , and (d)  $\lambda = 12.34 \mu\text{m}$ . The other parameters are  $E_{f1} = 0.4 \text{ eV}$ ,  $E_{f2} = E_{f3} = 0.5 \text{ eV}$ ,  $R = 100 \text{ nm}$ ,  $L = 300 \text{ nm}$ ,  $g = 50 \text{ nm}$ , and  $w = 40 \text{ nm}$ . (For interpretation of the references to color in this figure legend, the reader is referred to the web version of this article.)

and with merely graphene ring are also given. It can be seen from the black curve that if the upper graphene ring is removed, the resonant wavelengths of the first- and second-order transmission dips are about  $11.70 \mu\text{m}$  and  $7.62 \mu\text{m}$  with the two transmission dips both approaching to zero, which means that most of the field power can be trapped into the graphene strip at resonance. The red curve is for the case of removing the graphene strip, and one can see that the resonant wavelength of the first- and second-order transmission dips are about  $9.86 \mu\text{m}$  and  $7.16 \mu\text{m}$  at this time, and both the two dip transmissions are larger than 0.3. To sum up, both the two basic structures can act as optical bandstop filters. When the graphene ring and strip are used simultaneously, as is shown by the blue curve, two PIT windows occur in the transmission spectrum, one corresponding to the first-order resonance and the other to the second-order resonance. The new transmission dips on both sides of the first- and second-order PIT peaks are all close to zero. In addition, the wavelengths of the transmission dips on the left sides of the PIT windows are close to those of the structure with only graphene ring (red curve), while the wavelengths of transmission dips on the right sides of the PIT windows are close to those of the structure with only graphene strip (black curve). For the first order PIT window, the wavelengths of the two dips and the PIT peak are respectively about  $10.11 \mu\text{m}$ ,  $12.34 \mu\text{m}$  and  $10.73 \mu\text{m}$ . As for the second order PIT, they are about  $7.26 \mu\text{m}$ ,  $7.73 \mu\text{m}$ , and  $7.41 \mu\text{m}$ . In this paper, we mainly focus on the first order PIT, and the result for the second order one is similar. It will be proved that the left dip (marked as b) and the transparent window (marked as c) are mainly affected by the upper graphene ring resonator and its coupling with the graphene strip. And the right dip (marked as d) is relative to the graphene strip and its coupling with the upper graphene ring. This phenomenon can also be explained by the destructive interference of GSPs between two optical pathways [51,52]. In fact, the resonance in the graphene strip can be directly excited by the incident GSP wave from the graphene bus waveguide, while the resonance in the ring resonator can only be excited by the coupling of GSP wave from the strip resonator. Thus, the lower graphene strip acts as a bright resonator, while the upper ring behaves as a dark resonator. Then two optical pathways can be referred as graphene bus-strip-ring-strip and graphene bus-strip. As a result, the destructive interference of the GSP waves propagating between these two optical pathways will lead to the formation of PIT-like transparent window on the spectrum.

In order to give a deep insight into the physical mechanism behind the PIT-like effect, the distributions of the field component Hz for the proposed structure at wavelength  $10.11 \mu\text{m}$ ,  $10.73 \mu\text{m}$ , and  $12.34 \mu\text{m}$  corresponding to the points b, c and d in Fig. 5(a) are shown in

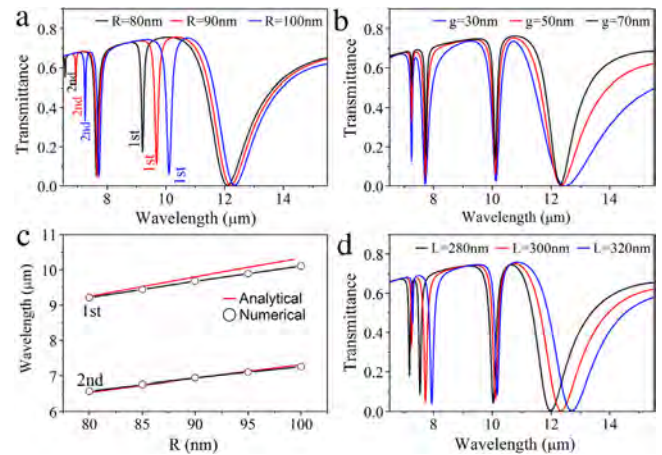


**Fig. 6.** (a) Transmission spectra for different values of  $R$  when  $g = 50 \text{ nm}$ , and  $L = 300 \text{ nm}$ . (b) Transmission spectra for different values of  $g$  when  $R = 100 \text{ nm}$ ,  $L = 300 \text{ nm}$ . (c) Simulation (black lines with circles) and theoretical results (red lines) of the resonant wavelength of the left dips of the first and second order PIT-like transparent windows as a function of the radius of the graphene ring. (d) Transmission spectra for different  $L$  when  $R = 100 \text{ nm}$ ,  $g = 50 \text{ nm}$ . The other parameters are  $E_{f1} = 0.4 \text{ eV}$ ,  $E_{f2} = E_{f3} = 0.5 \text{ eV}$ ,  $w = 40 \text{ nm}$ . (For interpretation of the references to color in this figure legend, the reader is referred to the web version of this article.)

Figs. 5(b), (c) and (d) respectively. It is well-known that for the graphene ring resonator, the phase matching condition for the formation of a standing wave at resonance can be described by the following equation [53,54]:

$$L_{eff} \times Re(neff) = m\lambda \quad (7)$$

where  $L_{eff} = 2\pi R$  is the perimeter of the graphene ring, and positive number  $m$  stands for the standing wave order. By using of Eq. (7) together with Eq. (6), one can find that the wavelength of point b in Fig. 5(a) is approximately satisfied with the condition of standing wave formation in the graphene ring with  $m = 1$ , and which will result in a strong field trap in the graphene ring as shown in Fig. 5(b). However, as can be seen from Fig. 5(c), destructive interference is formed in the graphene strip and only the dark graphene ring resonator is efficiently activated, while the bright graphene strip resonator is strongly suppressed [55]. Also GSP wave can be directly passed through the graphene bus waveguide, resulting in a PIT-like transparent window. In Fig. 5(d), the magnetic field is mainly distributed in graphene strip and is less on the graphene ring. This is mainly because  $\lambda = 12.34 \mu\text{m}$  is closer to the first-order resonance of the single graphene strip, and away from the resonant wavelength of the graphene ring. Furthermore, one can also find from Figs. 5(b) and (d) that the distributions of Hz in the graphene strip and the bus waveguide are out-of-phase, which will lead to the transmission dips b and d. Meanwhile, it can also be considered that the transmission dip d is mainly controlled by the graphene strip, while the dip b is relevant to the graphene ring.

To further understand the transmission characteristics of the proposed PIT waveguide on the structure parameters, we firstly fix the geometry parameters  $L = 300 \text{ nm}$ ,  $w = 40 \text{ nm}$  and  $g = 50 \text{ nm}$  but make the radius of the graphene ring  $R$  vary from 80 to 100 nm with a step of 10 nm so as to study the changes of the transmission spectrum and the results are shown in Fig. 6(a). It can be found that the overall transmission spectra are red shifted with the increase of radius  $R$ , which can be interpreted by Eq. (7), namely, the increase of radius  $R$  will lead to the increase of the perimeter of the graphene ring resonator, and thus the increase of its resonance wavelength. Meanwhile, the redshifts of the transmission dips on the left sides of the transparent windows are clearer than those on the right sides. As a result, the line width (FWHM) of the transparent windows decreases with the increase of  $R$ . In addition, it also certifies that the left dips are mainly controlled by

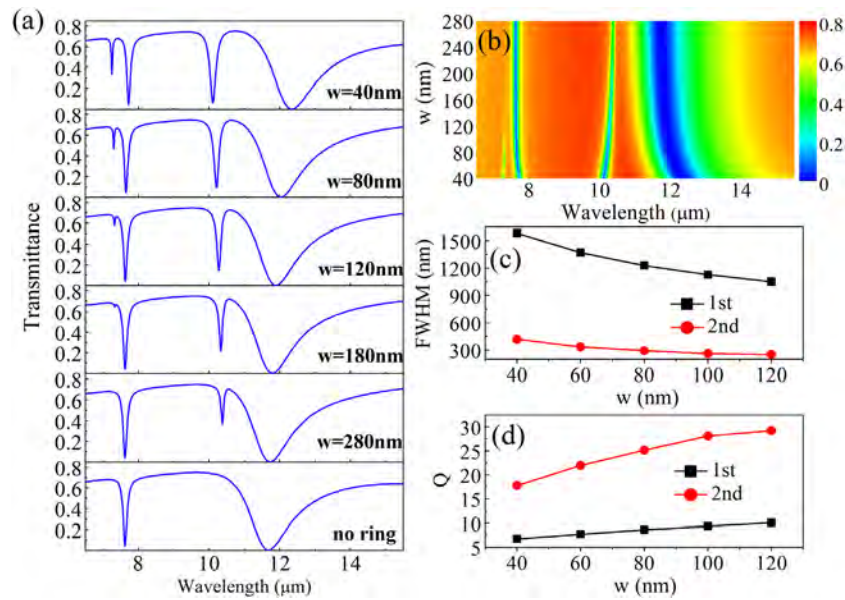


**Fig. 7.** (a) Transmission spectra for different values of  $w$ . (b) Pseudo color plot of transmission spectrum as a function of  $w$ . (c) FWHM and (d) Q factor extracted from the transmission spectra for different values of  $w$ . Here  $E_{f1} = 0.4$  eV,  $E_{f2} = E_{f3} = 0.5$  eV,  $R = 100$  nm,  $L = 300$  nm and  $g = 50$  nm. (For interpretation of the references to color in this figure legend, the reader is referred to the web version of this article.)

the graphene ring, and thus people can control the location and the line width of the transmission spectra by adjusting the graphene ring's radius in realizing the applications of filtering or other photonic devices. Next, the wavelength of the dips on the left sides of the transparent windows as a function of the graphene ring radius is shown in Fig. 6(c), which indicates a better agreement between the simulation results (black lines with circles) and the theoretical results (red lines) calculated by Eq. (7). The slight difference between the theory and the simulation results, especially for the first order resonant, is caused by the stronger coupling between the graphene strip and the ring. Yet the difference can be reduced by increasing the coupling distance  $w$  or taking the higher order resonance into consideration. Then, the influence of the gap  $g$  on the transmission spectra is shown in Fig. 6(b) with  $R = 100$  nm,  $w = 40$  nm and  $L = 300$  nm. It is clear that the resonance wavelengths are almost unchanged when  $g$  increases from 30 nm to 70 nm, but the maximal transmission ratio increases slightly due to the weakened coupling of the field power from bus waveguide to strip resonator. Fig. 6(d) shows the relationship between the transmission spectra and the length  $L$  of the graphene strip under the condition of  $g = 50$  nm,  $w = 40$  nm and  $R = 100$  nm. One can find that the positions of the PIT-like windows and the left transmission dips are very slightly red shifted with the increase of  $L$ , but the line widths of the transparent windows increase clearly with the increasing  $L$  due to the obvious redshift of the right dips. This further indicates that the right transmission dips are mainly controlled by the graphene strip resonator.

It is known that the formation of PIT-like effect of the proposed graphene-based waveguide structure is due to the existence of the stronger coupling between the bright resonator act by the graphene strip and the dark resonator act by the upper graphene ring. However, the interaction between the bright and the dark resonance is mainly controlled by the separation distance  $w$ . Studies of the transmission properties affected by the parameter  $w$  is shown in Fig. 7. It can be found that when  $w$  changes from 40 to 280 nm or even more, the transmission rate of left dips for both first and second order resonance will rise gradually, but their locations have no clear changes. When  $w = 280$  nm, the transparent window formed by second order resonance will disappear. The transparent window formed by the first order resonance will also disappear when  $w$  continues increasing. This is because the increase of  $w$  will lead to the weakened coupling between the graphene strip and the upper graphene ring resonator, and thus one of the optical

pathways (graphene bus-strip-ring-strip) is to be destroyed gradually. As a result, the GSPs power entering into the graphene ring resonator decreases, and the PIT-like transmission spectrum shifts gradually into the transmission spectrum of the waveguide structure composed of a graphene bus waveguide side-coupled with a single vertical graphene strip resonator. During this process, the dips on the right sides of the first-order transparent windows are clearly blue shifted, but there is no obvious change for those of the second-order one. All the results shown here again prove that the left transmission dips are mainly determined by the graphene ring resonator, and the stronger coupling between the graphene strip and ring will lead to the redshift of the right dips. Here the other parameters are the same as those in Fig. 5. To deepen the understanding of the result shown in Fig. 7(a), the pseudo color plot of the transmission spectra as a function of separation  $w$  is shown in Fig. 7(b), from which one can see the effect of  $w$  on the transmission spectra more intuitively. As a conclusion, the value of  $w$  can be an effective tuning factor in altering the line shape of the transmission spectra to present features of stopband filtering and PIT-like effects. Figs. 7(c) and (d) show the changes of FWHM [56] and the quality factor of the two transparent windows when  $w$  increases from 40 nm to 120 nm with a step of 20 nm. Here the quality factor of the transparent window is defined as  $Q = \lambda/\text{FWHM}$  and in which  $\lambda$  is the PIT peak wavelength. In Fig. 7(c), the FWHM of the two transparent windows decreases with the increase of  $w$ , and the FWHM value of the lower order PIT-like transparent window is more sensitive to  $w$  than that of the higher order one. The quality factor  $Q$  increases with the increase of  $w$ , as plotted in Fig. 7(d) because PIT peak wavelength of the transparent windows has almost no dependence on  $w$ . This result provides a possible way to control the PIT-like transparent window in real application.

As is known for the graphene-based plasmon waveguide, one of the greatest advantages is that one can change the chemical potential of graphene by applying external gate voltage to dynamically adjust the transmission properties. So the dependence of the transmission properties of the proposed PIT waveguide on the chemical potential will be investigated as following. At first, the transmission spectrum for different chemical potentials of graphene strip  $E_{f2}$  is studied by setting  $E_{f1} = 0.4$  eV and removing the graphene ring and the simulation result is given in Fig. 8(a). The other parameters are the same as those in Fig. 5. It can be seen from Fig. 8(a) that the transmission spectra are blue shifted with the increase of  $E_{f2}$  while the line shape is not affected.

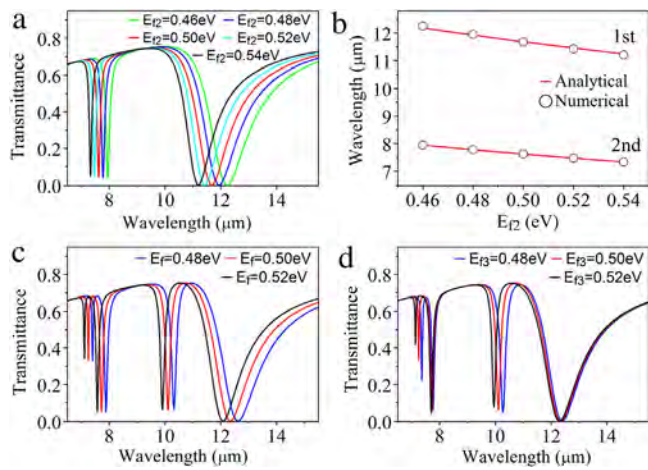


**Fig. 8.** (a) Transmission spectra without the upper graphene ring for various chemical potentials of the graphene strip  $E_{f2}$  when  $E_{f1} = 0.4$  eV. (b) Dependence of the resonant wavelength on  $E_{f2}$  when  $E_{f1} = 0.4$  eV. Red lines are the analytical results and black circles are the numerical results. (c) Transmission spectra with  $E_{f1} = 0.4$  eV when  $E_{f2} = E_{f3} = E_f$  is different. (d) Transmission spectra with  $E_{f1} = 0.4$  eV,  $E_{f2} = 0.5$  eV when the chemical potential of graphene ring  $E_{f3}$  is different. Here  $R = 100$  nm,  $L = 300$  nm,  $g = 50$  nm and  $w = 40$  nm. (For interpretation of the references to color in this figure legend, the reader is referred to the web version of this article.)

This can be also seen from Fig. 8(b), which further illustrates that the numerical results agree well with the theoretical fitting determined by Eq. (5). Secondly, the upper graphene ring resonator with chemical potential  $E_{f3}$  is added. Here,  $E_{f2} = E_{f3} = E_f$  is used and other parameters are the same as Fig. 8(a), and the transmission spectra of different  $E_f$  are shown in Fig. 8(c) in which the blue shift of the transmission spectrum is observed when  $E_f$  increases from 0.48 eV to 0.52 eV. Thirdly, take the  $E_{f2} = 0.5$  eV and the changed values of  $E_{f3}$ , the simulated transmission spectra are shown in Fig. 8(d). It is obvious that as the chemical potential of graphene ring  $E_{f3}$  increases, the transmission dips on the left sides of the PIT-like windows are blue shifted while the right dips have almost no changes. By adjusting the chemical potential of the graphene ring and strip respectively, one can dynamically tune the transmission dips and the PIT-like windows, and thus the proposed graphene-based PIT structure can work as a nanoscale plasmon filter or other functional devices without changing the size of the structure.

In order to broaden the applications of the proposed PIT waveguide structure, it is necessary to further study its transmission characteristics from the perspective of refractive index sensors. Practically, as an example, one can select the stopband on the left side of the first order PIT-like window as the working frequency band. The transmission properties will be investigated by filling the sample to be detected into the graphene ring resonator. For the aim of simplicity, the refractive index of the medium filled in the graphene ring is assumed to be  $n = 1.00$  to  $n = 1.05$  with a step of 0.01 during the numerical simulation, and the result is shown in Fig. 9. It can be seen from Fig. 9(a) that the transmission spectrum is red shifted obviously with the increase of medium index  $n$ , and the shift of the transmission dip is about to 208 nm when the refractive index  $n$  varies from 1 to 1.05, which means that the change of transmission spectrum is sensitive to the change of medium index  $n$ . Fig. 9(b) indicates that the dip wavelength of the transmission spectrum is linearly dependent on the increase of medium index  $n$ . This is helpful to design refractive index sensors by using graphene materials in the nanoscale. Fig. 9(c) reveals that the FWHM increases with the increase of the refractive index. It is well-known that the sensitivity and the figure of merit (FoM\*) are the two basic parameters for describing a nanoscale sensor. Here the sensitivity is defined as the ratio of the wavelength shift to the change of refractive index  $S = \delta\lambda/\delta n$  [57,58], which reflects the change of the resonance wavelength when

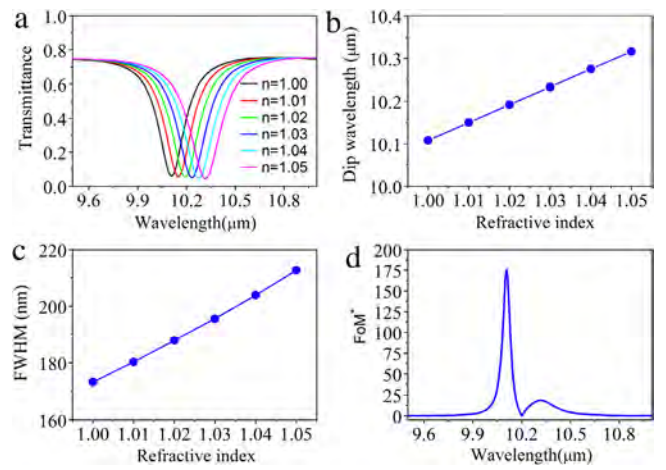


**Fig. 9.** (a) Transmission spectra with different refractive indexes of graphene ring. (b) Transmission dip wavelength with different refractive indexes. (c) The FWHM under different refractive indexes. (d) FoM\* as a function of working wavelength. Here  $E_{f1} = 0.4$  eV,  $E_{f2} = E_{f3} = 0.5$  eV,  $R = 100$  nm,  $L = 300$  nm,  $g = 50$  nm and  $w = 40$  nm.

the refractive index of the medium changes one unit and allows for the detection of a small refractive index change of the medium filled in the graphene ring resonator. Meanwhile, another comprehensive parameter of FoM\* used to evaluate the sensing performance is defined as  $\text{FoM}^* = \delta T / (T \delta n)$  [59], where  $T$  denotes the transmission in the proposed structure, and  $\delta T = |T(\omega, n + \delta n) - T(\omega, n)|$  is the variation of the transmittance at frequency  $\omega$  caused by refractive index change  $\delta n$ . The calculated sensitivity is as high as about 4160 nm/RIU in the wavelength range of 9.5–11.5  $\mu\text{m}$ , which is larger than that obtained in Refs. [32,60,61]. As shown in Fig. 9(d), when the refractive index changes from 1.00 to 1.05 with  $\delta n = 0.05$ , a obvious sensing response can be found at the wavelength of about 10.11  $\mu\text{m}$ , and the calculated result shows that the maximum FoM\* is about 175 at this time, which is superior to that of Ref. [62–64] and is beneficial for the design of nanoscale photonic sensors.

#### 4. Conclusion

In conclusion, a new type of graphene-based waveguide structure composed of a bus waveguide side coupled with a graphene strip resonator directly and with a graphene ring resonator indirectly has been proposed in this paper. The so-called PIT effect can be achieved by controlling the relevant parameters. The refractive index sensor is realized with a sensitivity of 4160 nm/RIU as well as a higher value of figure of merit. The presented waveguide structure and the features obtained for it can be useful in optical integrated circuits, especially in the design of nano sensors, switches, slow light devices, and modulators.

#### Acknowledgments

This work is supported by the Natural Science Foundation of Shanxi Province (Grant No. 2016011038) and the Natural Science Foundation of China (Grant No. 61475198, 61775126).

#### References

- [1] K.J. Boller, A. Imamoglu, S.E. Harris, Observation of electromagnetically induced transparency, *Phys. Rev. Lett.* 66 (20) (1991) 2593–2596.
- [2] S.H. Harris, Electromagnetically induced transparency, *Phys. Today* 50 (7) (1997) 36–42.
- [3] N. Liu, L. Langguth, T. Weiss, J. Kästel, M. Fleischhauer, Plasmonic analogue of electromagnetically induced transparency at the drude damping limit, *Nature Mater.* 8 (9) (2009) 758–762.

- [4] B. Luk'yanchuk, N.I. Zheludev, S.A. Maier, N.J. Halas, L. Peter, The Fano resonance in plasmonic nanostructures and metamaterials, *Nature Mater.* 9 (9) (2010) 707–715.
- [5] J.X. Chen, P. Wang, C.C. Chen, Y.H. Lu, H. Ming, Q.W. Zhan, Plasmonic EIT-like switching in bright-dark-bright plasmon resonators, *Opt. Express* 19 (7) (2011) 5970–5978.
- [6] A.H. Safavi-Naeini, T.P.M. Alegre, J. Chan, M. Eichenfield, M. Winger, J.T. Hill, Q. Lin, D. Chang, O. Painter, Electromagnetically induced transparency and slow light with optomechanics, *Nature* 472 (7341) (2011) 69–73.
- [7] F. Arya, P.C. Julien, Design of tunable bi-periodic graphene metasurfaces, *Phys. Rev. B* 86 (19) (2012) 195408–195409.
- [8] J.C. Wang, X.Y. Liang, S.X. Xia, S.T. Liu, Tunable multimode plasmon-induced transparency with graphene side-coupled resonators, *Jpn. J. Appl. Phys.* 55 (2) (2016) 022201–022206.
- [9] C. Hu, L.L. Wang, Q. Lin, X. Zhai, X.Y. Ma, T. Han, J. Du, Tunable double transparency windows induced by single subradiant element in coupled graphene plasmonic nanostructure, *Appl. Phys. Express* 9 (5) (2016) 052001–052004.
- [10] G.L. Fu, X. Zhai, H.J. Li, S.X. Xia, L.L. Wang, Tunable plasmon-induced transparency based on bright-bright mode coupling between two parallel graphene nanostrips, *Plasmonics* 11 (6) (2016) 1597–1602.
- [11] L. Wang, W. Li, X. Jiang, Tunable control of electromagnetically induced transparency analogue in a compact graphene-based waveguide, *Opt. Lett.* 40 (10) (2015) 2325–2328.
- [12] K.S. Novoselov, A.K. Geim, S.V. Morozov, D. Jiang, Y. Zhang, S.V. Dubonos, Electric field effect in atomically thin carbon films, *Science* 306 (5696) (2004) 666–669.
- [13] K.S. Novoselov, A.K. Geim, S.V. Morozov, D. Jiang, M.I. Katsnelson, I.V. Grigorieva, S.V. Dubonos, A.A. Firsov, Two-dimensional gas of massless Dirac fermions in graphene, *Nature* 438 (7065) (2005) 197–200.
- [14] Z.Y. Fang, Y.M. Wang, A.E. Schlather, Z. Liu, P.M. Ajayan, F.J.G. de Abajo, P. Nordlander, X. Zhu, N.J. Halas, Active tunable absorption enhancement with graphene nanodisk arrays, *Nano Lett.* 14 (1) (2014) 299–304.
- [15] Y.C. Fan, N.H. Shen, T. Koschny, C.M. Soukoulis, Tunable terahertz meta-surface with graphene cut-wires, *ACS Photon.* 2 (2015) 115–156.
- [16] X.S. Wang, C. Chen, L. Pan, J.C. Wang, A graphene-based Fabry-Pérot spectrometer in mid-infrared region, *Sci. Rep.* 6 (2016) 32616.
- [17] J. Wei, Z.G. Zang, Y.B. Zhang, M. Wang, X.S. Tang, Enhanced performance of light-controlled conductive switching in hybrid cuprous oxide/reduced graphene oxide (Cu<sub>2</sub>O/rGO) nanocomposites, *Opt. Lett.* 42 (5) (2017) 911–914.
- [18] Z.G. Zang, X.F. Zeng, M. Wang, W. Hu, C.R. Liu, X.S. Tang, Tunable photoluminescence of water-soluble AgInZnS-graphene oxide (GO) nanocomposites and their application in-vivo bioimaging, *Sensors Actuators* 252 (2017) 1179–1186.
- [19] H.G. Yan, X.S. Li, B. Chandra, G. Tulevski, Y.Q. Wu, M. Freitag, W.J. Zhu, P. Avouris, F.N. Xia, Tunable infrared plasmonic devices using graphene/insulator stacks, *Nat. Nanotechnol.* 7 (2012) 330–334.
- [20] Y. Zhao, G.X. Chen, Z.C. Tao, C.Y. Zhang, Y.W. Zhu, High Q-factor plasmonic resonators in continuous graphene excited by insulator-covered silicon gratings, *RSC Adv.* 4 (2014) 26535–26542.
- [21] X.Y. He, P.Q. Gao, W.Z. Shi, A further comparison of graphene and thin metal layers for plasmonics, *Nanoscale* 8 (19) (2016) 10388–10397.
- [22] A. Vakil, N. Engheta, Transformation optics using graphene, *Science* 332 (6035) (2011) 1291–1294.
- [23] H.Y. Zhang, Y.Y. Cao, Y.Z. Liu, Y. Li, Y.P. Zhang, A novel graphene metamaterial design for tunable terahertz plasmon induced transparency by two bright mode coupling, *Opt. Commun.* 391 (2017) 9–15.
- [24] Z. Fei, A.S. Rodin, G.O. Andreev, W. Bao, A.S. McLeod, M. Wagner, L.M. Zhang, Z. Zhao, M. Thiemens, G. Dominguez, M.M. Fogler, A.H. Castro Neto, C.N. Lau, F. Keilmann, D.N. Basov, Gate-tuning of graphene plasmons revealed by infrared nano-imaging, *Nature* 487 (5) (2012) 82–85.
- [25] J.N. Chen, M. Badioli, P. Alonso-González, S. Thongrattanasiri, F. Huth, J. Osmond, M. Spasenović, A. Centeno, A. Pesquera, P. Godignon, A.Z. Elorza, N. Camara, F.J.G. de Abajo, R. Hillenbrand, F.H.L. Koppens, Optical nano-imaging of gate-tunable graphene plasmons, *Nature* 487 (5) (2012) 77–81.
- [26] M. Grande, G.V. Bianco, M.A. Vincenti, D. De Ceglia, P. Capezzuto, V. Petruzzelli, M. Scalora, G. Bruno, A. D’Orazio, Optically transparent microwave screens based on engineered graphene layers, *Opt. Express* 24 (20) (2016) 22788–22795.
- [27] L. Wu, H.S. Chu, W.S. Koh, E.P. Li, Highly sensitive graphene biosensors based on surface plasmon resonance, *Opt. Express* 18 (14) (2010) 14395–14400.
- [28] H. Cheng, S.Q. Chen, P. Yu, X.Y. Duan, B.Y. Xie, J.G. Tian, Dynamically tunable plasmonically induced transparency in periodically patterned graphene nanostrips, *Appl. Phys. Lett.* 103 (20) (2013) 203112–203114.
- [29] X.S. Wang, X.S. Xia, J.C. Wang, F. Zhang, Z.D. Hu, C. Liu, Tunable plasmonically induced transparency with unsymmetrical graphene-ring resonators, *J. Appl. Phys.* 118 (1) (2015) 013101–013105.
- [30] Y.K. Wang, X.R. Shen, Q.S. Chen, Tunable plasmon-induced transparency with graphene-sheet structure, *Modern Phys. Lett. B* 30 (19) (2016) 1650232–1650238.
- [31] M.T. Wen, L.L. Wang, X. Zhai, Q. Lin, S.X. Xia, Dynamically tunable plasmon-induced absorption in resonator-coupled graphene waveguide, *Europhys. Lett.* 116 (2016) 44004–44006.
- [32] S.X. Xia, X. Zhai, L.L. Wang, B. Sun, J.Q. Liu, S.C. Wen, Dynamically tunable plasmonically induced transparency in sinusoidally curved and planar graphene layers, *Opt. Express* 24 (16) (2016) 17886–17889.
- [33] X.S. Xia, J.C. Wang, F. Zhang, Z.D. Hu, C. Liu, X. Yan, L. Yuan, Multi-mode plasmonically induced transparency in dual coupled graphene-integrated ring resonators, *Plasmonics* 10 (2015) 1409–1415.
- [34] J.C. Wang, X.S. Wang, H.Y. Shao, Z.D. Hu, G.G. Zheng, F. Zhang, Peak modulation in multicavity-coupled graphene-based waveguide system, *Nanoscale Res. Lett.* 12 (2017) 9.
- [35] Q. Lin, X. Zhai, L.L. Wang, B.X. Wang, G.D. Liu, S.X. Xia, Combined theoretical analysis for plasmon-induced transparency in integrated graphene waveguides with direct and indirect couplings, *Europhys. Lett.* 111 (2015) 34004–34006.
- [36] J.C. Wang, C. Song, J. Hang, Z.D. Hu, F. Zhang, Tunable Fano resonance based on grating coupled and graphene-based otto configuration, *Opt. Express* 25 (20) (2017) 23880–23892.
- [37] Y. Zhang, L.Y. Zhang, C.W. Zhou, Review of chemical vapor deposition of graphene and related applications, *Acc. Chem. Res.* 46 (10) (2013) 2329–2339.
- [38] K.Y. Li, G. Eres, J. Howe, Y.J. Chuang, X.F. Li, Z.J. Gu, L.T. Zhang, S.S. Xie, Z.W. Pan, Self-assembly of graphene on carbon nanotube surfaces, *Sci. Rep.* 3 (2013) 2353.
- [39] B.K. Min, S.K. Kim, S.J. Kim, S.H. Kim, M.A. Kang, C.Y. Park, W. Song, S. Myung, J.S. Lim, K.S. An, Electrical double layer capacitance in a graphene embedded Al<sub>2</sub>O<sub>3</sub> gate dielectric Si, *Sci. Rep.* 5 (2015) 16001.
- [40] Y.X. Gao, G.B. Ren, B.F. Zhu, J. Wang, S.S. Jian, Single-mode graphene-coated nanowire plasmonic waveguide, *Opt. Lett.* 39 (20) (2014) 5909–5912.
- [41] J.C. Wang, B.J. Tang, X.S. Xia, S.T. Liu, Active multiple plasmon-induced transparency with graphene sheets resonators in mid-infrared frequencies, *J. Nanomater.* 2016 (2016) 3678578.
- [42] J.P. Liu, X. Zhai, L.L. Wang, H.J. Li, F. Xie, Q. Lin, S.X. Xia, Analysis of mid-infrared surface plasmon modes in a graphene-based cylindrical hybrid waveguide, *Plasmonics* 11 (3) (2016) 703–711.
- [43] Y. Francescato, G. Vincenzo, S.A. Maier, Strongly confined gap plasmon modes in graphene sandwiches and graphene-on-silicon, *New J. Phys.* 15 (6) (2013) 063020.
- [44] Z.R. Huang, L.L. Wang, B. Sun, M.D. He, J.Q. Liu, H.J. Li, X. Zhai, A mid-infrared fast-tunable graphene ring resonator based on guided-plasmonic wave resonance on a curved graphene surface, *J. Opt.* 16 (10) (2014) 105004–105007.
- [45] G. Gumbs, A. Lurov, J.Y. Wu, M.F. Lin, P. Fekete, Plasmon excitations of multilayer graphene on a conducting substrate, *Sci. Rep.* 6 (2016) 21063.
- [46] T.J. Constant, S.M. Hornett, D.E. Chang, E. Hendy, All-optical generation of surface plasmons in graphene, *Nature Phys.* 12 (2) (2016) 124–128.
- [47] Q. Li, T. Wang, Y.K. Su, M. Yan, M. Qiu, Coupled mode theory analysis of mode-splitting in coupled cavity system, *Opt. Express* 18 (8) (2010) 8367–8382.
- [48] H. Lu, Plasmonic characteristics in nanoscale graphene resonator-coupled waveguides, *Appl. Phys. B* 118 (1) (2015) 61–67.
- [49] H.S. Chu, C.H. Gan, Active plasmonic switching at mid-infrared wavelengths with graphene ribbon arrays, *Appl. Phys. Lett.* 102 (23) (2013) 231107.
- [50] J. Christensen, A. Manjavacas, S. Thongrattanasiri, F.H.L. Koppens, F.J.G. de Abajo, Graphene plasmon waveguiding and hybridization in individual and paired nanoribbons, *ACS Nano* 6 (1) (2011) 431–440.
- [51] Y. Huang, L.W. Ma, M.J. Hou, Z.J. Zhang, Universal near-field interference patterns of Fano resonances in two-dimensional plasmonic crystals, *Plasmonics* 11 (5) (2016) 1377–1383.
- [52] Z.D. Zhang, R.B. Wang, Z.Y. Zhang, J. Tang, W.D. Zhang, C.Y. Xue, S.B. Yan, Electromagnetically induced transparency and refractive index sensing for a plasmonic waveguide with a stub coupled ring resonator, *Plasmonics* 12 (4) (2017) 1007–1013.
- [53] B. Wang, G.P. Wang, Plasmonic waveguide ring resonator at terahertz frequencies, *Appl. Phys. Lett.* 89 (13) (2006) 133106.
- [54] K.H. Wen, Y.H. Hu, L. Chen, J.Y. Zhou, M. He, L. Lei, Z.M. Meng, Plasmonic-induced absorption and transparency based on a compact ring-groove joint mim waveguide structure, *IEEE Photon. J.* 8 (5) (2016) 4802308–4802309.
- [55] T. Wang, Y.S. Zhang, Z. Hong, Z.H. Han, Analogue of electromagnetically induced transparency in integrated plasmonics with radiative and subradiant resonators, *Opt. Express* 22 (18) (2014) 21529–21534.
- [56] S.W. Luo, B. Li, D.S. Xiong, D.L. Zuo, X.B. Wang, A high performance plasmonic sensor based on metal-insulator-metal waveguide coupled with a double-cavity structure, *Plasmonics* 12 (2) (2017) 223–227.
- [57] K.H. Wen, Y.H. Hu, L. Chen, J.Y. Zhou, L. Lei, Z.M. Meng, Single/dual Fano resonance based on plasmonic metal-dielectric-metal waveguide, *Plasmonics* 11 (1) (2016) 315–321.
- [58] W. Wei, J.P. Nong, L.L. Tang, G.W. Zhang, J. Yang, W. Luo, Conformal graphene-decorated nanofluidic sensors based on surface plasmons at infrared frequencies, *Sensors* 16 (6) (2016) 899.

- [59] H. Lu, X.M. Liu, D. Mao, G.X. Wang, Plasmonic nanosensor based on Fano resonance in waveguide-coupled resonators, *Opt. Lett.* 37 (18) (2012) 3780–3782.
- [60] S.X. Xia, X. Zhai, Y. Huang, J.Q. Liu, L.L. Wang, S.C. Wen, Graphene surface plasmons with dielectric metasurfaces, *J. Lightw. Technol.* 35 (20) (2017) 4553–4558.
- [61] S.X. Xia, X. Zhai, L.L. Wang, J.P. Liu, H.J. Li, J.Q. Liu, A.L. Pan, S.C. Wen, Excitation of surface plasmons in graphene-coated nanowire arrays, *J. Appl. Phys.* 120 (2016) 103104–103109.
- [62] W. Wei, J.P. Nong, G.W. Zhang, Y. Zhu, An infrared biosensor based on graphene plasmonic for integrated nanofluidic analysis, *Proc. SPIE* 9278 (2014) 92780F.
- [63] N. Liu, M. Mesch, T. Weiss, M. Hentschel, H. Giessen, Infrared perfect absorber and its application as plasmonic sensor, *Nano. Lett.* 10 (2010) 2342–2348.
- [64] X.C. Yan, T. Wang, Z.X. Han, S.Y. Xiao, Y.J. Zhu, Y.B. Wang, High sensitivity nanoplasmonic sensor based on plasmon-induced transparency in a graphene nanoribbon waveguide coupled with detuned graphene square-nanoring resonators, *Plasmonics* 12 (5) (2017) 1449–1455.